High Efficacy of Panobinostat Towards Human Gastrointestinal Stromal Tumors in a Xenograft Mouse Model

Giuseppe Floris,[1] Maria Debiec-Rychter,[2] Raf Sciot,[3] Cristiana Stefan,[1] Steffen Fieuws,[4] Kathleen Machiels,[2] Peter Atadja,[5] Agnieszka Wozniak,[1] Gavino Faa,[6] and Patrick Schöffski[1]

Abstract

Purpose: Histone deacetylase inhibitors have emerged as potent anticancer compounds. Using a nude-mouse xenograft model, for the first time we evaluated the response of human gastrointestinal stromal tumors (GIST) carrying different oncogenic *KIT* mutations to panobinostat (LBH589), administered single or in combination with imatinib.

Experimental Design: We grafted the human GIST882 cell line with *KIT* exon 13 mutation and two biopsies from patients radiologically progressing under imatinib showing *KIT* exon11 and *KIT* exon9 mutations, respectively. Our study included 4 groups: A (n = 9; control), B (n = 10; panobinostat 10 mg/kg daily, i.p.), C (n = 9; imatinib 150 mg/kg bidaily, p.o), and D (n = 8; combination panobinostat-imatinib, same dose/schedule as above). Treatment lasted 12 days. Tumor size was measured regularly using standard variables. Histopathological assessment was by H&E, and immunohistochemically with KIT, cleaved caspase-3, Ki-67, and histone acetylation staining.

Results: Overall, GIST xenografts responded rapidly to panobinostat as indicated by tumor regression, necrosis, hemorrhages, fibrosis, and/or myxoid degeneration, remarkable apoptosis, and substantial decline of cell proliferation. H3 and H4 acetylation increased significantly from control level in all treated groups. The combination of panobinostat and imatinib further enhanced most of the assessed parameters.

Conclusions: We show for the first time potential therapeutic activity of panobinostat in human GISTs, *in vivo*. Our results warrant further exploration of histone deacetylase inhibitors for the treatment of advanced GISTs. Our study is also the first one on human GIST mouse xenografts established using patient biopsies.

Authors' Affiliations: [1]Department of General Medical Oncology and Laboratory of Experimental Oncology, Departments of [2]Human Genetics, and [3]Pathology, University Hospital Gasthuisberg, and [4]I-BioStat, KU Leuven and University of Hasselt, Leuven, Belgium; [5]Novartis Institutes for Biomedical Research, Cambridge, Massachusetts; and [6]Department of Pathology, University of Cagliari, Istituto di Anatomia Patologica, Cagliari, Italy

Received 10/13/08; revised 1/24/09; accepted 3/28/09; published OnlineFirst 6/9/09.

Grant support: G. Floris received a grant from the Autonomous Region of Sardinia (Italy) in the frame of "Master and Back Project" (project # TS152). This work is supported by research grants from the Life Raft Group, from the Fonds voor Wetenschappelijk Onderzoek Vlaanderen (FWO grant # G. 0510.06 P. Schöffski and # G.0286.05 M. Debiec-Rychter) and by a Concerted Action Grant 2006/14 from the K.U.Leuven. P. Atadja is employed by Novartis Pharmaceuticals, whose drugs were studied in the present work. The costs of publication of this article were defrayed in part by the payment of page charges. This article must therefore be hereby marked *advertisement* in accordance with 18 U.S.C. Section 1734 solely to indicate this fact.

Note: Supplementary data for this article are available at Clinical Cancer Research Online (http://clincancerres.aacrjournals.org/).

Requests for reprints: Giuseppe Floris, Department of General Medical Oncology and Laboratory of Experimental Oncology, University Hospital Gasthuisberg, Catholic University of Leuven, Herestraat 49, bus 815; 3000 Leuven, Belgium. Phone: 32-0-16346900; Fax: 32-0-16346901; E-mail: giuseppe.floris@med.kuleuven.be.

doi:10.1158/1078-0432.CCR-08-2588

Gastrointestinal stromal tumors (GIST) are the most common mesenchymal cancers of the digestive system, showing resistance to radiotherapy and/or conventional chemotherapy (1). They have heterogeneous pathoclinical features and behavior, ranging from benign to overtly malignant sarcomas with spindle cell, epithelioid cell, or mixed-cell component (2, 3). GISTs are driven mainly by oncogenic mutations in the KIT receptor, also known as CD117 or stem cell factor receptor (4). *KIT* exon 11 mutations are the most frequent (70-85%), whereas *KIT* exon 9 mutations account for 5% to 15% of cases (5). The tyrosine kinase inhibitor imatinib mesylate targeting KIT has been a major breakthrough in the treatment of patients with advanced GISTs (1). However, in time, most patients experience drug resistance, clinically classified as primary (early, within 6 months of therapy) or secondary (late; ref. 6). Secondary *KIT* mutations account most frequently for this resistance, followed by amplification of the *KIT* gene (7, 8). Alternative GIST therapies after failure to imatinib are, as yet, only in development (6, 9).

Histone deacetylase (HDAC) inhibitors (HDACi) are long known in psychiatry and neurology as mood stabilizers and antiepileptics (10). However, in the past decades, they emerged as potent anticancer compounds with antiproliferative and proapoptotic activities (11). HDACi may primarily act through the transcriptional reactivation of dormant tumor suppressor

Translational Relevance

The data presented in this study show that panobinostat (LBH589; pan-HDAC-inhibitor of a new generation) has strong antitumor potential against gastrointestinal stromal tumors (GIST), and in combination with imatinib, the therapeutic effect is enhanced. Protein lysine acetylation is emerging as a proper signaling system influencing various functions in different cellular compartments including apoptosis and protein folding (cytoplasm), and gene expression (nucleus). Thus, pan-HDAC inhibitors offer a wide range of appealing anticancer targets, and emerge as ideal compounds to be associated in standard cancer therapy. The elucidation of the heterogeneous molecular mechanism conferring resistance to imatinib in GISTs renders the need for novel therapeutic strategies of utmost importance. The combined therapy with imatinib (membrane) and histone deacetylase inhibitors (cytoplasm+nucleus) represents a promising strategy for the treatment of patients with advanced GISTs, potentially overcoming resistance to imatinib.

genes (11). Their targets, histone deacetylases, are involved in tumorigenesis through either aberrant recruitment to promoters or enhanced expression, resulting in histone deacetylation and transcription repression (12). Nonhistone proteins, such as HSP90, are also HDAC substrates, and the antitumor effect of HDACi is attributed to transcription-independent mechanisms as well (12, 13). The inhibition of the cytoplasmatic HDAC6 by HDACi including LBH589 leads to acetylation of HSP90 and reduced affinity for its client proteins, which are subsequently poliubiquinated and degraded by the proteasome (14, 15). HSP90 activity has been implicated in the activation and maturation of mutant KIT oncoproteins in GIST cell lines (16).

HDACi belong to unrelated classes of compounds such as short-chain fatty acids, hydroxamic acids, benzamides, cyclic tetrapeptides, and ketones, and inhibit the Zn^{2+}-dependent histone deacetylases of class I and II through direct interaction with the active Zn^{2+} in the catalytic site (17, 18). One particular feature of HDACi is that they preferentially kill transformed or neoplastic cells and are relatively nontoxic to normal cells *in vivo* and *in vitro* (11). The basis for this selective toxicity is not fully understood.

With the more recent approval of vorinostat, a pan-HDACi, for the treatment of refractory cutaneous T-cell lymphomas, the epigenetic-based therapy through HDAC inhibition opens a new avenue for cancer treatment (18). Vorinostat was also shown to display strong antiproliferative and proapoptotic effects in both sensitive and imatinib-resistant GIST cell lines (19). Other HDACi currently in clinical development for various hematological or solid tumors include panobinostat, belinostat, romidepsin, MS-275, and MGCD0103 (18, 20–23). In combination with classic chemotherapeutic drugs or other targeted therapies, HDACi hold promises for improved cancer therapy (24).

Panobinostat (LBH589; Novartis Pharma AG) is a hydroxamic acid derivative. The drug was reported to potentiate the action of anticancer agents such as bortezomib, dexamethasone, or melphalan but also to overcome drug resistance in multiple myeloma cells (25).

In the present study, we evaluated in a xenograft mouse model the anticancer potency of panobinostat, alone or in combination with imatinib, toward three malignant human GISTs carrying different primary *KIT* oncogenic mutations. We show for the first time that panobinostat treatment is highly effective, resulting in significant tumor shrinkage, arrest of tumor cell proliferation and enhanced apoptosis.

Materials and Methods

Chemicals and drugs. Antibodies to p-Y703 KIT (mc), cleaved caspase-3 (D175; mc), acetyl-K9 histone 3 (Ac-H3K9; pc), acetyl-K18 histone 3 (Ac-H3K18; pc), acetyl-K8 histone 4 (Ac-H4K8; pc), acetyl-K12 histone 4 (Ac-H4K12; pc), p-S473 AKT (pc), AKT (pc), p-T202/Y204 mitogen-activated protein kinase (MAPK; pc), p42/44 MAPK (pc) *STAT3* (pc), *pY705 STAT3* (pc), and *FOXO3a* (pc) were from Cell Signaling. Antibodies to B-actin (pc), α-tubulin (clone DM1A; mc), and acetylated α-tubulin (clone 6-11B-1; mc) were from Sigma-Aldrich. Antibodies to Ki-67 (clone SP6; mc) were from Thermo Scientific. Antibodies to KIT (CD117; pc), horseradish peroxidase (HRP)-polyclonal rabbit anti-mouse immunoglobulins, HRP-polyclonal goat anti-rabbit immunoglobulins, the anti-rabbit Envision+ System-HRP–labeled polymer, and 3′-diaminobenzidine-tetrahydrochloride were from DAKO. Western Lightning chemiluminescence reagent was from Perkins and Elmer. Bio-Rad protein assay and the polyvinylidene difluoride membranes were from Bio-Rad. Electrophoresis was carried in NuPAGE gels from Invitrogen. Imatinib mesylate (Glivec/Gleevec) and the cinnamic acid hydroxamate panobinostat (LBH589) were provided by Novartis Pharma AG.

Cell line, biopsies, and mice. The GIST882 cell line carrying the homozygous *KIT* exon 13 K642E (*KIT*-exon13) mutation was a kind gift from Dr. Jonathan Fletcher (Department of Pathology, Brigham and Women's Hospital, Harvard Medical School, Boston, MA; ref. 26). GIST biopsies with heterozygous *KIT* exon 9 A502_Y503dup (*KIT*-exon9) and *KIT* exon 11 K558_G565delinsR (*KIT*-exon11) mutations, respectively, were obtained from patients radiologically progressing under imatinib. Female adult athymic NMRI nude mice (36-42 grams) were obtained from Janvier laboratories.

Generation of mouse GIST xenografts. Heterotopic GISTs xenografts were generated by subcutaneous inoculations of GIST 882 cells as previously described (27), or s.c. transplantation of biopsies on both sides. We retransplanted the tumors when they reached 0.7 to 1 cm^3 volume (8-12 wk). At each passage, a tumor piece was snap frozen in liquid nitrogen and another one fixed in formalin. For this study, we used 10 mice with GIST882 (4th passage), 12 mice with *KIT*-exon9 (3rd passage), and 14 mice with *KIT*-exon11 (4th passage) mutations.

Experimental design and treatment. All animal experiments were approved by the ethical committee of the Catholic University of Leuven. Thirty-six mice, each bearing 2 GIST xenografts (except for 1 mouse with 3 tumors, and 2 mice with one tumor) of (average) ~700 mm^3 were assigned to 4 treatment groups: not treated (group A), panobinostat (group B), imatinib (group C), and panobinostat-imatinib combination (group D). Imatinib was administered orally by gavages at 150 mg/kg twice a day, and LBH589 i.p at a 10mg/kg daily. The treatment lasted 12 d. Mice were randomly assigned to the four groups. Group A composed of 16 tumors (4 *KIT*-exon13, 8 *KIT*-exon11, and 4 *KIT*-exon9 mutants). Group B composed of 21 tumors (6 *KIT*-exon13, 9 *KIT*-exon11, and 6 *KIT*-exon9 mutants). Group C composed of 18 tumors (6 *KIT*-exon13, 6 *KIT*-exon11, and 6 *KIT*-exon9 mutants). Group D included 16 tumors (4 *KIT*-exon13, 6 *KIT*-exon11, and 6 *KIT*-exon9 mutants). After treatment initiation, tumor volume and mice body weight were assessed at baseline, day 4th, 8th, and 12th of the experiment. Three orthogonal diameters were measured with Vernier

caliper, and the ellipsoid formula was used to calculate tumor volume (28). When treatment ended, pieces of tumor were either fixed in 10% buffered formalin, or snap frozen in liquid nitrogen. Organs, including liver, kidney, lung, spleen, and intestine were collected for treatment side effect evaluation.

Histology. Paraffin sections (5 μm) were cut for H&E staining and immunohistochemistry. Mitoses and apoptotic bodies were counted in 10 high power fields (HPF) at 400-fold magnifications. Ki-67 labeling index was calculated as the average percentage of Ki-67–positive nuclei in three HPF. Apoptotic activity was confirmed and measured from cleaved caspase-3 immunostaining. Acetylation status of different lysines in histones H3 and H4 was calculated as the percentage of positive nuclei in three HPF. Histologic response was graded based on the microscopic amount of necrosis, myxoid degeneration or fibrosis using previously proposed grading scheme: 1, minimal (0-10%); 2, low (>10% and ≤50%); 3, moderate (>50% and ≤90%); and 4, high (>90%) grade, respectively (29). Microscopy was with Olympus LH-30M, pictures were taken with Olympus digital camera Color View, and analysis was done with Olympus Cell D imaging software.

Immunoblotting. Tumor lysates were obtained from frozen tissue, as described (7), and used for immunoblot analysis. Electrophoresis was done in NuPAGE 4-12% Bis-tris gels from Invitrogen, and chemiluminescence was captured with the FUJI mini-LAS3000-plus imaging system.

Sequencing. Mutational analysis was done on patient biopsies and on randomly chosen 36 xenografts (3 tumors per genotype from each experimental group). Genomic DNA was extracted from frozen biopsies or from neoplastic areas from paraffin sections using the High Pure PCR Template Preparation kit (Roche). *KIT* exon 9, 11, 13, 14, and 17 were screened for mutations, using a combination of PCR amplification, denaturing high-performance liquid chromatography, and bidirectional sequencing, as described before (30).

Fluorescence* in situ *hybridization. Dual-color interphase fluorescence *in situ* hybridization (FISH) was done on 36 paraffin sections selected as mentioned above. Digoxigenin-labeled BACs RP11-568A2 DNA for *KIT* were cohybridized with SpectrumGreen-labeled chromosome 4 centromeric probe (CEP4; Vysis, Inc.), as described (7). The FISH data were collected on a Leica DMRB (Leica) fluorescence microscope equipped with a cooled black and white charged couple camera (Photometrics), run by Quips SmartCapture FISH Imaging Software (Vysis). One hundred interphase nuclei were evaluated, and the ratio of *KIT*/CEP4 was calculated. A ratio of >2 was defined as *KIT* amplification.

Statistics. A general linear model with three factors (time, group genotype) was used to compare the changes in tumor volume from baseline. The main interest was in the comparison at 12 d. Due to a right-skewed distribution, volume values were first logarithmically transformed. Consequently, ratios were obtained after back-transformation to the original scale. Because each mouse was measured repeatedly over time and contributed at least two tumors, the statistical model included the possible correlations between the repeated measures. Thus, we considered a random effect from mouse and applied a heterogeneous compound symmetrical covariance matrix for the measurements over time. The model was fitted using the statistical procedure PROC MIXED (SAS, version 9.1). A Poisson regression model was used to compare the counts of mitosis, apoptosis, and the cleaved-caspase3 between the four groups. The differences between groups were allowed to be genotype specific. Generalized estimating equations were used to deal with the multiple tumors per mouse. Finally, a general linear model was used to compare the Ki-67 labeling index and the mean global histone-acetylation between groups. The differences between groups were also allowed to be genotype specific. The data were logarithmically transformed, and the variances were allowed to be specific for each genotype/group combination. Computationally, it was not feasible to add a random mouse effect to take into account the correlation between the tumors within a mouse. P values of <0.05 were considered statistically significant.

Results

Effect of treatment on tumors growth. We obtained 71 GIST xenografts: 20 with *KIT*-exon13, 29 with *KIT*-exon11, and 22 with *KIT*-exon9 mutations. Having been assigned to the study groups, treatment lasted 12 days, with dose schedules as described in Materials and Methods. Overall, the tumors in the control group grew steadily from baseline (Fig. 1A), showing ~2-fold increase at day 12. On average at day 12, both single treatments resulted in tumor shrinkage with 25% and 62% reduction under panobinostat and imatinib, respectively (Fig. 1A). This response was further increased under the combination schedule (73% reduction; Fig. 1A). After 12 days, the differences among the 4 groups were highly statistically significant ($P < 0.0001$). The changes in the tumor volume related significantly to *KIT* genotype ($P < 0.0001$). Thus, in group A, *KIT*-exon11 xenografts showed the highest increase in volume from baseline (Fig. 1B). In group B (panobinostat), the *KIT*- exon11 mutants remained rather steady in size, showing 106% of the baseline volume on day 12 [95% confidence interval (95% CI), 81-139%; Fig. 1B)]. By contrast, the *KIT*-exon9 and *KIT*-exon13 xenografts had a 37% volume reduction from baseline at day 12. This result is significantly different in comparison with control tumors ($P = 0.0016$ and $P < 0.0001$ respectively; Fig. 1C and D). In group C (imatinib), the *KIT*- exon11 xenografts showed the most remarkable response, with 80% reduction from baseline (Fig. 1B). This response was significantly different from the responses of *KIT*-exon13 and *KIT*-exon9 mutants ($P < 0.0001$), which regressed only by 45% and 50% from baseline, respectively (Fig. 1C and D). In addition, the difference in response between imatinib and panobinostat-treated mice with GISTs carrying *KIT*-exon11 mutation was highly significant ($P < 0.0001$). In GISTs with *KIT*-exon13 and *KIT*-exon9 mutations, these differences were not statistically significant ($P = 0.49$ and $P = 0.32$, respectively).

In group D (combination), on day 12, the best response was in the *KIT*-exon13 and *KIT*-exon11 xenografts (~80% reduction; Fig. 1B and D), whereas in the *KIT*-exon9 mutants, the reduction was of 56% (Fig. 1C). However, only in the GIST882 tumors, there was statistical evidence for an added effect of the combined therapy in comparison with imatinib alone ($P < 0.0001$).

Genotype and FISH analysis. We confirmed the presence of the original *KIT* genotype in all selected xenografts, but we did not identify any secondary mutations in *KIT* exon 13, 14, or 17, neither in the original samples (biopsies) nor in the grafts. However, the *KIT*-exon 9 xenografts shifted their *KIT* status from heterozygous to homozygous. Control xenografts bearing *KIT*-exon11 and *KIT*-exon13 mutations showed diploid copy number of the *KIT* gene in majority of nuclei (mean KIT/nucleus ratio 2.3 and 1.9, respectively). In line with genotyping, *KIT*-exon9 xenografts revealed only one copy of the *KIT* gene in the majority of cells (mean *KIT*/nucleus ratio, 1.35; mean *KIT*/CEP4 ratio, 0.9). The *KIT* copy number remained unchanged, regardless of the treatment. Also, no *KIT* amplification was recorded in any of the analyzed specimens.

Histopathology assessment. Macroscopically, all xenografts were multinodular with no infiltration of surrounding tissues (Table 1). Microscopically (H&E staining), the *KIT*-exon9 and

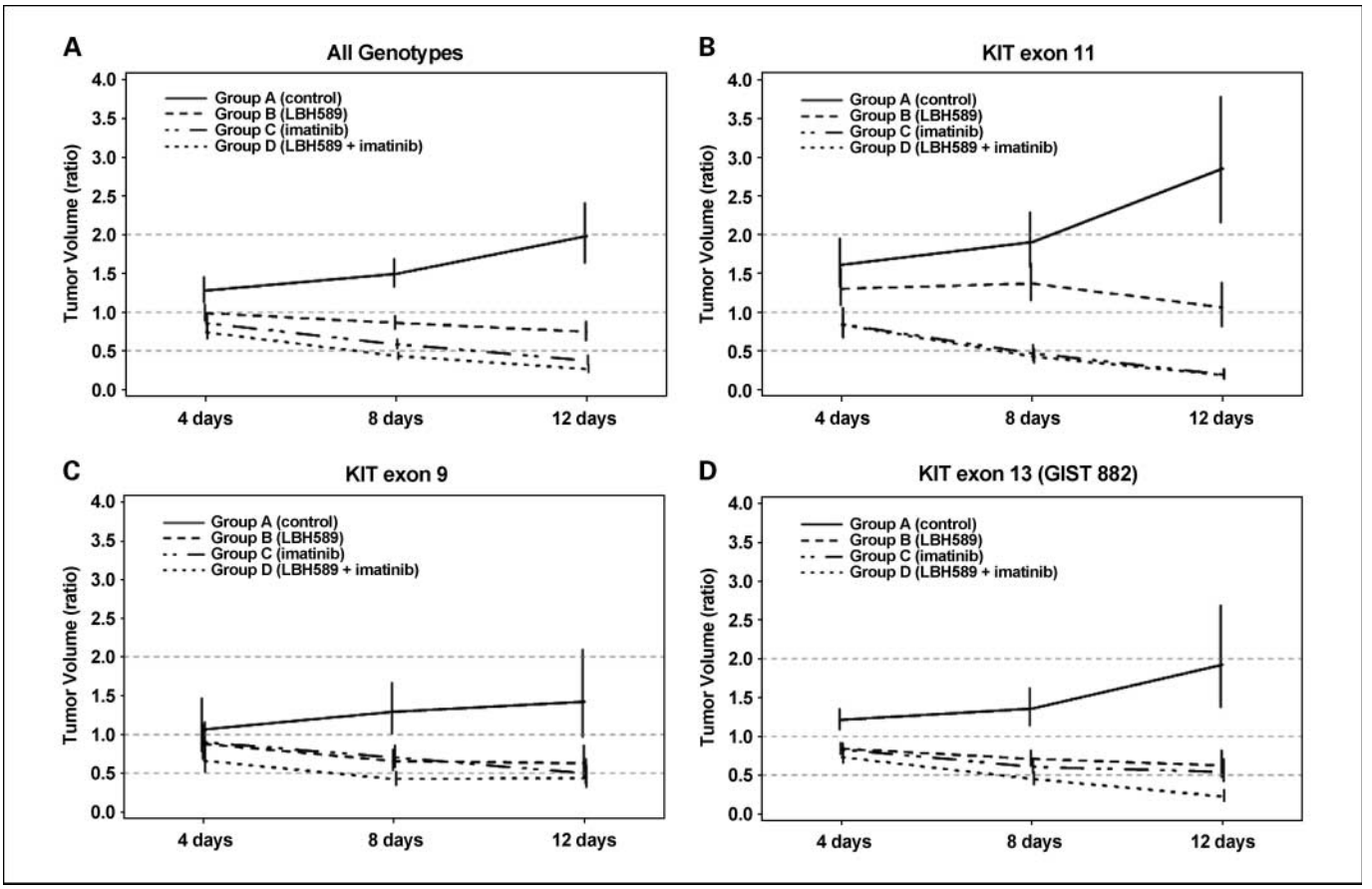

Fig. 1. Tumor volume. Tumor volume was assessed at baseline (control) and on day 4, 8, and 12 of treatment. Values were right skewed; therefore, data were processed as described in Materials and Methods. For each time point, averages and 95% CIs are plotted. Tumor growth assessment was evaluated regardless of genotype (*A*), in GIST *KIT* exon 11 (*B*), *KIT* exon 9 (*C*), and *KIT* exon 13 (*D*).

KIT-exon11 tumors showed mixed population of epithelioid and spindled cells, whereas the GIST882 ones were composed mainly of spindled cells. KIT immunostaining was cytoplasmic, with diffuse pattern in all three types of xenografts, and somewhat weaker staining in the GIST 882 derived-tumors.

A histologic response (H&E) including myxoid degeneration, necrosis, calcification, scarring, and ischemia (31) was found in all xenografts, regardless of *KIT* mutation and treatment. However, this response was heterogeneous in grade and did not correlate with tumor volume reduction (Fig. 2A). Panobinostat alone induced the best response, grade 1 to 3, in GIST882 and *KIT*-exon11 tumors (Fig. 2A). By contrast, *KIT*-exon9 xenografts showed only grade 1 response under panobinostat. Overall, panobinostat induced wide areas of necrosis and small foci of microscopic necrosis in the majority of the *KIT*-exon11 and GIST882 xenografts (Fig. 2B and C). In addition, the GIST882 tumors showed myxoid degeneration, calcifications, and ischemia often associated with blood vessels lined by a hyalinized vessel wall (Fig. 2D). Grade 1 to 3 response, with no grade 4, was also observed in group C (imatinib; Fig. 2A). GIST882-derived tumors showed a more heterogeneous response (grade 1-3) than *KIT*-exon9 and *KIT*-exon11 xenografts, which scored, all but one, only grade 1 (Fig. 2A). We identified grade 4 histologic response only in group D (combination), in two GIST882 and one *KIT*-exon11 tumors (Fig. 2A). Here, histologic changes were overall identical to those observed in group B (panobinostat), except for a more prominent myxoid degeneration in the GIST882 tumors.

We identified brisk mitotic activity in all tumor types in group A (control), ranging from 23 to 38 mitoses/10 HPF, with (average) 28 mitoses/10 HPF (95% CI, 27.02-29.96), clearly indicating high degree of malignancy (Fig. 3A). Overall, we found decreased mitotic activity or increased apoptotic activity in all three treatment groups. Under panobinostat, the mitotic activity, as estimated from H&E staining, decreased significantly ($P < 0.0001$) from (average) 28.5 mitosis/10 HPF in the control group to (average) 12.8 mitoses/10 HPF (95% CI, 10.8-15.2), whereas apoptotic count increased ($P < 0.0001$) from (average) 13.8 apoptotic bodies/10 HPF (95% CI, 12.3-15.3) to (average) 35 apoptotic bodies/10 HPF (95% CI, 30.1-40.9; Fig. 3A). The Ki-67 labeling index ($P < 0.0001$) as well as the apoptosis marker cleaved-caspase3 ($P < 0.0001$) confirmed the findings from H&E staining (Fig. 3B and C). When different genotypes were considered the mitotic index (H&E) decreased by ~2.5-fold in *KIT*-exon9 and in GIST882-derived tumors, and by 1.7-fold in the *KIT*-exon11 ones (Fig. 3A). The apoptotic activity (H&E) increased in all xenografts, by 3.2-fold in GIST882 and *KIT*-exon11 tumors, and 1.6-fold in *KIT*-exon9 tumors compared with nontreated ones (Fig. 3A). Some tumors treated with panobinostat alone showed a unique feature, i.e., scattered mitotically active cells with cytoplasm positive for cleaved-caspase3 (data not shown).

Overall, imatinib (group C) reduced ($P < 0.0001$) the mitotic activity to (average) 2.7 mitosis/10 HPF (95% CI, 1.9-3.8; Fig. 3A). Apoptotic activity increased ($P < 0.0001$) to (average) 33.4 apoptosis/10 HPF (95% CI, 27-41.3; Fig. 3A), as calculated from H&E staining. This increase was further confirmed by the immunostaining for cleaved-caspase3 ($P = 0.0008$; Fig. 3C). As shown by Ki-67 immunostaining, the reduction in the proliferative activity in group C was at least 2-fold higher in the GIST882 and *KIT*-exon11 tumors than in the *KIT*-exon9 ones (Fig. 3B). Apoptotic activity increased by 6.5-fold in *KIT*-exon11 GISTs, whereas in the remaining tumors, the increment ranged from 1.2 to 1.7 (Fig. 3A).

The mitotic activity decreased ($P < 0.0001$) during combination treatment (group D) to (average) 2.7 mitoses/10 HPF (95% CI, 2-3.6; Fig. 3A). Ki-67 immunostaining further confirmed the decreased proliferation in this group (13-fold; $P < 0.0001$; Fig. 3B). The increase in apoptosis under combination treatment was, however, the most remarkable of all three treatment groups, i.e., to (average) 97 apoptotic bodies/10 HPF (95% CI, 87.5-107.5; $P < 0.0001$; Fig. 3A). This notable increase was also confirmed by the caspase-3 immunostaining, which indicated (average) ~4-fold increase in comparison with controls ($P < 0.0001$; Fig. 3C). As in group C, the proliferative activity was affected to a higher degree in GIST882 and KIT-exon11 tumors than in the *KIT*-exon9 ones (Fig. 3A and B). The apoptotic activity was highest in *KIT*-exon11 derived tumors (30-fold increase in comparison with controls; Fig. 3A). In GIST882 and *KIT*-exon9–derived tumors, the increase was 8.3- and 1.4-fold, respectively (Fig. 3A).

KIT presence was confirmed in all control xenografts by immunostaining (data not shown).

Evaluation of histone and tubulin acetylation. It is well-known that HDACi enhance acetylation of the core histones (3). We further evaluated H3 and H4 acetylation by immunohistochemistry with four antibodies against acetylated lysine: Lys9 and Lys18 of H3, and Lys8 and Lys12 of H4. From each study group, we randomly chose nine tumors, with three tumors included for each genotype. The peroxidase reaction was exclusively nuclear (Fig. 4A). The histone acetylation pattern was mainly granular in control animals. The nuclei of the treated tumors looked more homogeously stained, partially hiding the granular appearance, most probably a reflection of chromatin rearrangements after enhanced histone acetylation.

We also did semiquantitative evaluation of the stained nuclei (Fig. 4B). For each section, three HPFs were selected for nuclear count, and the values for each antibody were pooled to obtain a mean global H3 and H4 acetylation status. In control tumors, on average, 57% of the nuclei showed H3 and H4 acetylation (95% CI, 53.55-60.34; Fig. 4B). Both the positive nuclei number and the nuclear staining intensity increased significantly in all treatment groups in comparison with the control one (at least $P = 0.0002$ for the 3 pair-wise comparison). Surprisingly, this increase was similar in group B (panobinostat) and group C (imatinib), up to 68% (95% CI, 65.94-69.28) and 66% (95% CI, 63.31-67.82), respectively, but was more prominent in group D (combination), up to 75%, (95% CI, 69.37-80.69), indicating an additional effect of combined treatment on histone acetylation ($P < 0.01$; Fig. 4B).

Interestingly, we found that the level of global acetylation in control tumors was significantly influenced by the genotypes ($P < 0.0001$). Thus, the GIST882 tumors showed higher level of acetylation (64%; 95% CI, 59.41-67.76) than the *KIT*-exon 11 (53%; 95% CI, 49.91-56.26) and *KIT*-exon 9 (54%; 95% CI, 45.43-62.9) ones. Panobinostat alone significantly increased the level of acetylation only in the GIST882 and GIST *KIT*-exon11 tumors ($P = 0.0004$ and $P < 0.0001$, respectively). Imatinib increased significantly the level of acetylation in *KIT*-exon9 ($P = 0.009$) and exon11–derived ($P < 0.0001$) GISTs, whereas in GIST882 tumors, the levels were not significantly affected ($P = 0.6$). Similarly to imatinib, the global acetylation status was significantly enhanced by the combination treatment only in *KIT*-exon9 ($P = 0.0001$) and *KIT*-exon11 ($P = 0.005$) tumors. This finding could be related to intrinsic biological differences of the three different genotypes but may require confirmation in a larger group.

HDAC6 is one of the panobinostat targets, and α-tubulin is one of the main substrate of this enzyme. Therefore, it was suggested that increased level of acetylated tubulin could be a surrogate marker for the cytoplasmic activity of panobinostat

Table 1. Macroscopic and microscopic characteristic of the GIST xenografts

Xenograft	Macroscopic appearance	Microscopic appearance (H&E)	KIT immunostaining
KIT exon 11–derived tumors	Multinodular growth pattern, no infiltration of surrounding tissues. In treated tumors, areas of hemorrhages, necrosis, and calcifications were observed*	Spindled cells arranged in cellular whorls or in "onion bulb–like" formations, making up multiple nodules rimmed by thin vessels. At the periphery of the sections, small nests of epithelioid cells with clear cytoplasm were observed	Strong and diffuse cytoplasmtic; focally membranous staining
KIT exon 9–derived tumors		Spindled cells arranged in short intersecting fascicles with abrupt transition toward epithelioid areas	Strong and diffuse, cytoplasmatic "Golgi-like" pattern
GIST882-derived tumors		Spindled cells arranged in short fascicles, showing a transition from hypercellular areas to hypocellular areas embedded in a myxoid stroma; scattered pleomorphic cells with enlarged hyperchromatic nuclei were observed as well	Weak and diffuse cytoplasmatic staining; focally "Golgi-like" pattern observed in some cases

*Macroscopic appearance description is the same for all three zenografts.

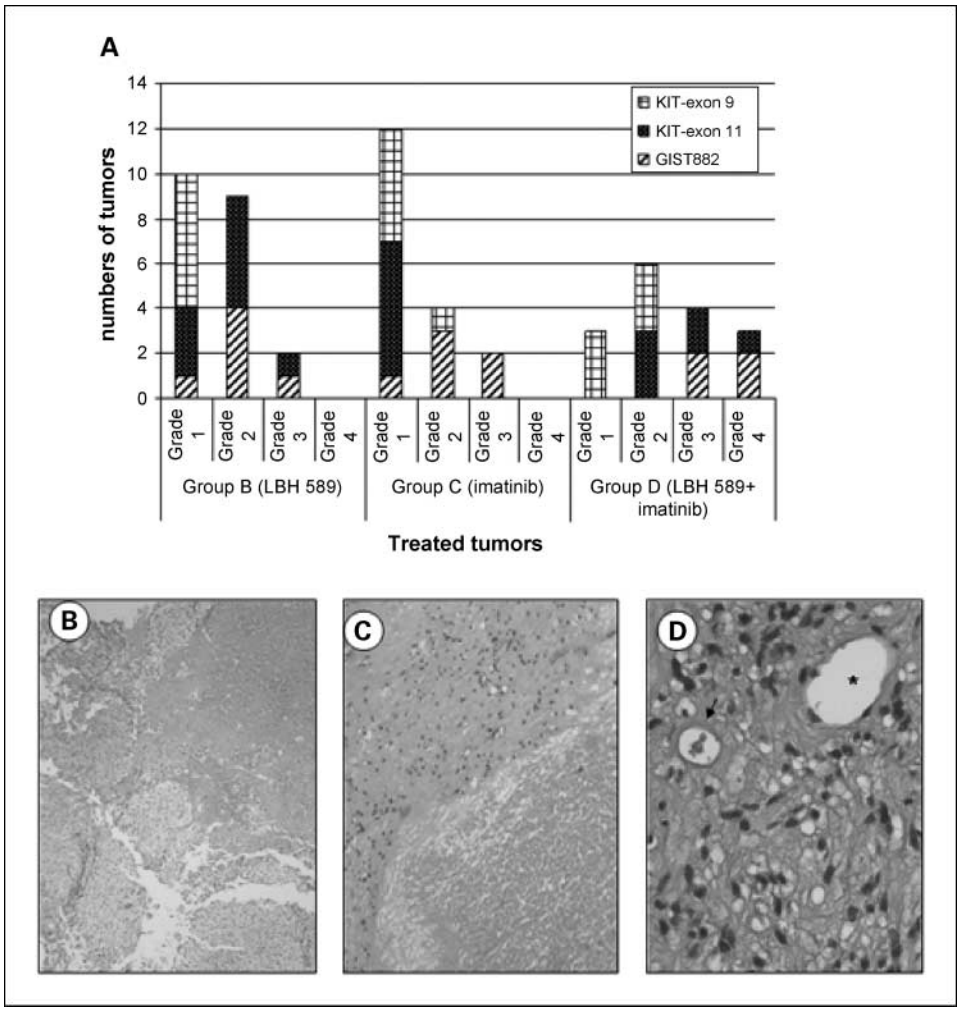

Fig. 2. Grading of the histologic response: *A,* grading was estimated as described in Materials and Methods. The GIST882-derived tumors responded best to therapy in all treatment groups. In the *KIT*-exon9 tumors, the histologic response was never higher than grade 2. In the *KIT*-exon11 tumors, the histologic response was heterogeneous, showing the best response under panobinostat (group B) and panobinostat + imatinib (group D). Grade 4 histologic response was observed only in the panobinostat-imatinib combination. *B,* under panobinostat, wide areas of necrosis shown by H&E (×40) were observed frequently in the *KIT*-exon11 and GIST882 tumors, and sometimes in coexistence with (*C*) myxoid degeneration. *D,* scattered "ghost vessels" characterized by hyalinization of the vessel wall (*arrow*) were identified in the GIST882 tumors (H&E; ×400); *, a normal vessel lined by flattened endothelium.

(12). To verify this hypothesis, we did immunoblot analysis in a substantial number of tumors (n = 35). However, overall, we did not find significant increases in α-tubulin acetylation in the panobinostat-treated tumors over control levels (Fig. 5A, B, and C). The specificity of the α-tubulin antibody was verified in a test study with primary GIST cells exposed for 24 hours to increased panobinostat concentrations (Supplementary Fig. S1). In this study, KIT expression and activation decreased under panobinostat in a dose-dependent manner.

Evaluation of KIT signaling pathways. Western analysis of total KIT in 35 tumors confirmed our findings from immunohistochemistry that KIT level significantly decreased only in the GIST882 tumors under combination treatment (Fig. 5).

In group A (control), the KIT phosphorylation level varied among genotypes, and even within same genotype, thus showing high heterogeneity. Notably, *KIT*-exon9 xenografts showed the strongest KIT phosphorylation. AKT was preferentially activated in tumors bearing *KIT*-exon11 and *KIT*-exon9 mutations, and negligible in GIST882-derived tumors. MAPK activation was weak, particularly in *KIT*-exon11 mutants.

Panobinostat did not influence KIT phosphorylation and its downstream molecules after 12-day treatment. Surprisingly, KIT phosphorylation did not change substantially under imatininb, regardless of xenograft genotype. However, we found changes in the activation of downstream AKT and MAPK in most tumors. In *KIT*-exon11 xenografts, AKT phosphorylation was significantly decreased in all specimens analyzed (Fig. 5A, *lanes 7-9*), whereas in *KIT*-exon 9 mutant tumors, a slight reduction of the phosphorylation level was observed only for MAPK (Fig. 5B, *lanes 8-9*). In GIST882 tumors, a more convincing reduction of the level of AKT and MAPK phosphorylation under imatinib was observed only in one tumor (Fig. 5C, *lane 7*).

In group D (combination), KIT and downstream molecule phosphorylation was significantly reduced in *KIT*-exon11 and GIST882 tumors. In the *KIT*-exon9 ones, a slight reduction in phosphorylation was found only for MAPK (Fig. 5B, *lanes 10-11*).

Total signal transducers and activators of transcription 3 (STAT3) was expressed in all xenografts, but it was not activated in control tumors, and no changes in the phosphorylation level were observed in the treated tumors (data not shown).

We further studied by immunohistochemistry the expression of the transcription factor FOXO3a, a protein downstream of AKT and important modulator of the cell cycle and apoptosis (32). It is generally accepted that the activity of FOXO3a is primarily regulated by its subcellular localization, being active in nucleus and inactive in the cytoplasm (32). In control tumors, FOXO3a was diffusely expressed mainly in the nuclei. In the KIT-exon11 and GIST882 tumors, FOXO3a staining appeared frequently also in the cytoplasm. In the KIT-exon9 ones, the protein

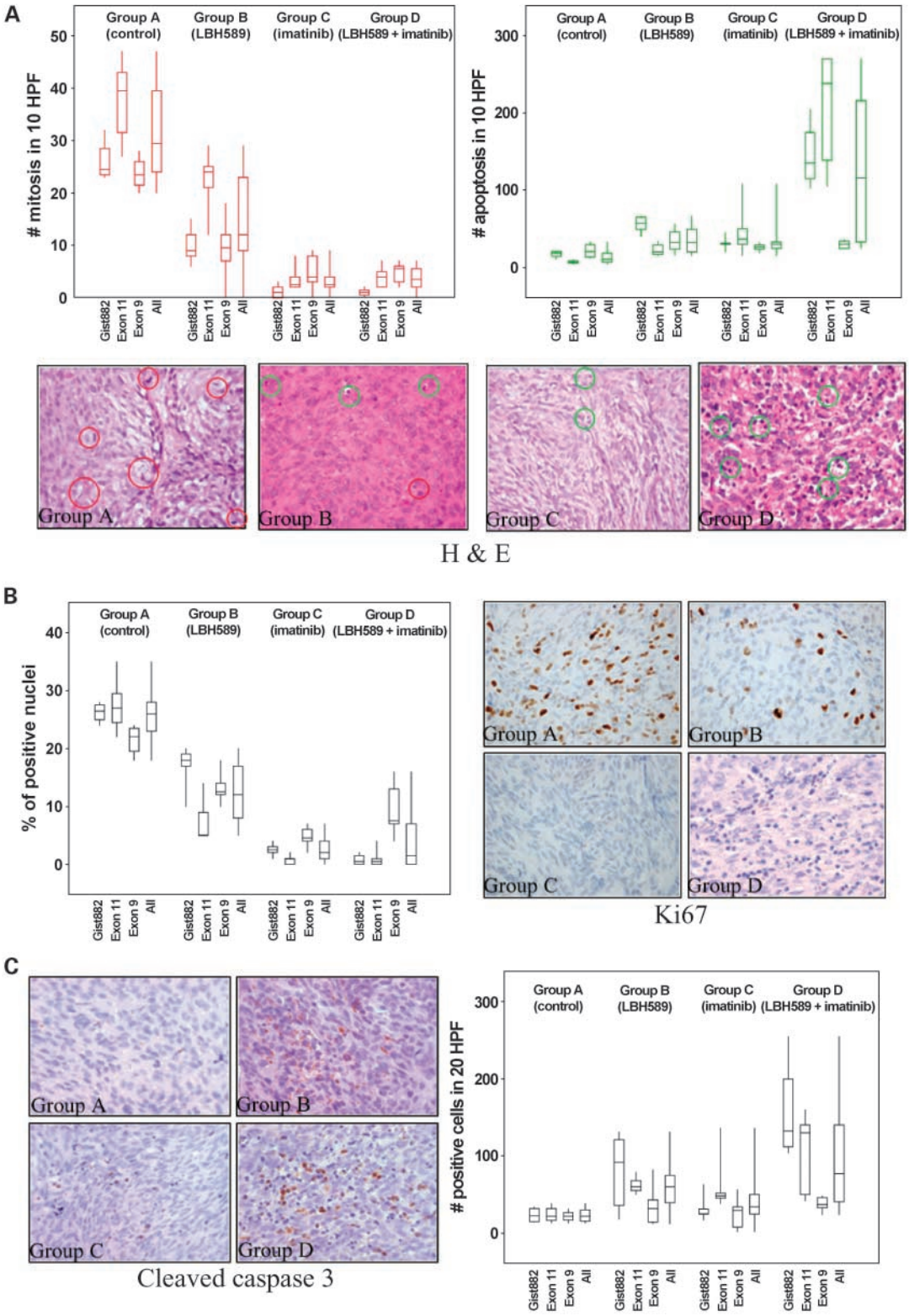

Fig. 3. Histopathologic assessment of the mitotic and apoptotic activity. Mitoses and apoptotic bodies in H&E stainings (*A*), positive nuclei for Ki-67 (*B*), and positive cells for cleaved-caspase3 (*C*) were counted as described in Materials and Methods. Results are presented as box plots showing minimum, maximum, and interquartile range. Within each treatment-group, the data are shown to illustrate the different GIST genotypes and all the tumors pooled together. Representative pictures for each staining and each group are also presented (H&E, Ki-67, and cleaved-caspase3). Mitosis (*red circles*) and apoptosis (*green circles*; H&E) are show in *A*.

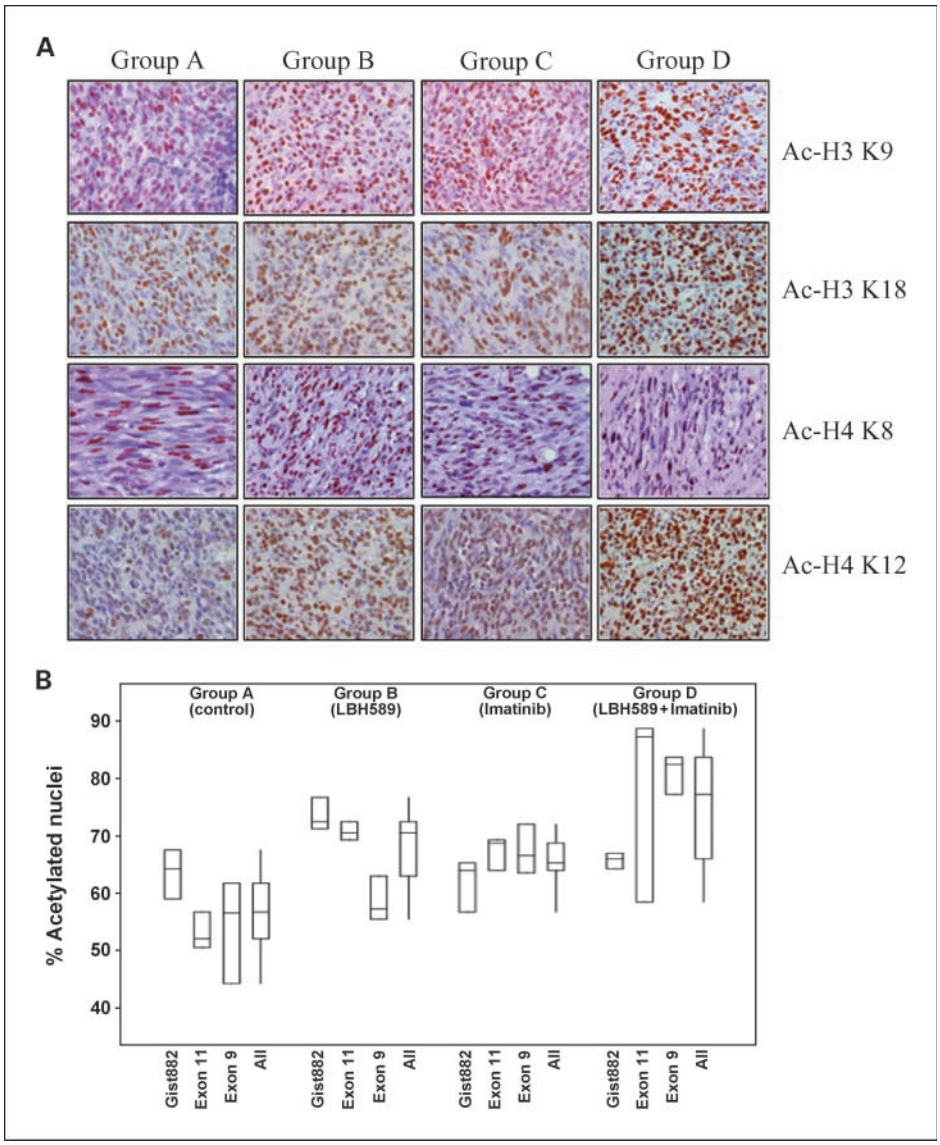

Fig. 4. Evaluation of H3 and H4 acetylation by immunohistochemistry. *A,* acetylation of specific Lys residues (Lys9 and Lys18 of H3, Lys8 and Lys12 of H4) was done in 36 specimens chosen randomly (9 for each group), and representative pictures are shown. *B,* the box plots showing minimum, maximum, and interquartile range are shown. For each staining, counts of positive nuclei were done in three HPFs per section, and averaged. For each specimen, the counts of the four staining were pooled to obtain a total acetylation status (H3 + H4). Within each treatment-group, the data are shown to illustrate the different GIST genotypes and all the tumors pooled together. Both panobinostat and imatinib treatment alone led to higher core histone acetylation than that in the control group. The combination treatment further increased the level of H3 and H4 acetylation.

was exclusively nuclear. However, the pattern of FOXO3a expression was unaffected by the different treatments in the three xenografts (Supplementary Fig. S2).

Treatment side effects. After 12-day treatment, the body weight decreased by 21% under panobinostat (group B). In group D (combination), the decrease was more pronounced (27%). In some of these animals, there was also skin dehydration and diarrhea. Histopathologically, panobinostat induced mild to moderate changes particularly in the spleen (dysplastic megakaryocytes) and in the small bowel (focal shortening of the villi).

Under imatinib (group C), the body weight was only slightly affected (7% reduction). A mild skin rash occurred only in some mice during the first days of drug administration. Liver, spleen, kidneys, and bowel showed no histologic alterations.

Discussion

Using a nude-mouse xenograft model, we show for the first time the antitumor activity of the HDACi panobinostat in three GISTs carrying distinctive oncogenic *KIT* mutations. Xenografts were obtained with the imatinib-sensitive GIST882 cell line or with biopsies from progressive patients on imatinib. According to the high mitotic index, all xenografts were highly aggressive. Mice received a 12-day treatment with panobinostat, imatinib, or combination of these drugs.

All GIST xenografts responded rapidly to panobinostat, early after treatment initiation. Panobinostat reduced significantly proliferation and increased apoptosis in all xenografts. Although nonhistone proteins are also HDAC substrates, the core histones are still their most abundant targets; therefore, their acetylation is a reliable marker for the HDACi bioavailability and activity (12). Indeed, the panobinostat-treated tumors showed a much stronger nuclear H3 and H4 acetylation as well as a higher number of positive nuclei than the control ones. We also found significant differences ($P < 0.0001$) in the basal H3 and H4 acetylation of the control tumors with different *KIT* mutants, with GIST882 tumors having the highest level. The global-acetylation status of the core histones might be related to differences in the biology of different

tumors as already described in prostatic (33) and lung carcinomas (34).

HDACi were shown to induce growth arrest and/or apoptosis to a variable extent both *in vitro* and *in vivo*, depending on the dose level (12, 35). The cell cycle is arrested at the G_1-S check point, but this activity does not necessarily depend on the apoptotic program activation. In our study, panobinostat did not completely abolish cell proliferation but clearly up-regulated their apoptotic activity. Interestingly, we also observed few cells in mitosis showing cleaved-caspase3 immunostaining. This finding is in line with the hypothesis that histone hyperacetylation of the pericentromeric heterochromatin occurring in the presence of HDACi leads to abnormal chromosomal segregation, nuclear fragmentation, and cell death due to aberrant mitosis (11). In accordance with this theory, we observed a trend toward a higher number of hyperacetylated mitoses in LBH589-treated mice than in the control ones (data not shown). However, mechanisms other than acetylation/deacetylation may promote or maintain the condensed state of the chromatin during mitosis (36).

As observed for other HDACi of the hydroxamate class, most likely panobinostat acts not only in the nucleus but also in the cytoplasm, through HDAC6 inhibition (12). By modulating the acetylation status of proteins such as α-tubulin and HSP90, HDAC6 is emerging as a master regulator of crucial cellular functions including the maturation of oncogenic protein kinases (37). Our experiment with cultured primary GIST cells showed that acetylated α-tubulin level is a marker for HDACi cytoplasmatic activity (12). However, in our *in vivo* study on xenografts, panobinostat did not significantly alter the level of the acetylated α-tubulin, suggesting that under our experimental conditions, such marker is not sensitive enough to prove the cytoplasmic activity of the drug. Cell exposure to HDACi leads to HSP90 acetylation, resulting in inhibition of its chaperone function and degradation of client proteins including the oncogenic KIT (14, 16). Indeed, as indicated by *in vitro* evidence and by our control experiment, after HDACi exposure, KIT expression is consistently impaired (19). In our xenografts, KIT level was only partially affected; therefore, it is conceivable that *in vivo* other mechanisms such as other post translational modifications modulate at different levels HSP90 activity (13). Furthermore, HDAC6 has been recently involved in the control of angiogenesis by stabilizing the hypoxia-inducible factor HIF-1α (13). We found focal areas of ischemia and scattered "ghost" vessels lined by a hyalinized wall, as indicated by H&E staining. This effect might be related to the antiangiogenic activity of panobinostat and, therefore, to its cytoplasmic activity. However, such features were only observed in the GIST882 tumors, suggesting that panobinostat mechanism of action may be heterogeneous and dependent on intrinsic biological features of individual tumors.

All GIST xenografts in our study significantly shrinked under imatinib, indicating they were all sensitive to the drug, although the *KIT*-exon11 and *KIT*-exon9 xenografts were obtained from biopsies of patients radiologically progressive under imatinib. The reason of their disease progression is not clear. We could not detect any secondary, imatinib-resistant *KIT* mutations, nor *KIT* amplification, which are the most frequent mechanisms for imatinib resistance in GISTs (7, 8). One explanation for the loss of resistance to imatinib can be that clones of imatinib-sensitive tumor cells are still present in the biopsies of these patients, and may have a better proliferation capacity in a new host and under imatinib withdrawal; therefore, they kept expanding from passage to passage in the nude mice. We consider the possibility that our xenografts still contained imatinib-resistant GIST clones, but the experiment did not last long enough to prove or exclude their presence. To our knowledge, our study is the first one done on mouse xenografts established with human GIST tumors rather than with cell lines, and successfully transferred for several passages. Therefore, it is difficult to relate this current finding to previous ones. Our study highlights once more the complexity of the imatinib resistance as well as of the GIST biology (38).

Notably, in spite of remarkable tumor shrinkage and pronounced histologic response under imatinib, KIT remained phosphorylated in all imatinib-treated xenografts. This is

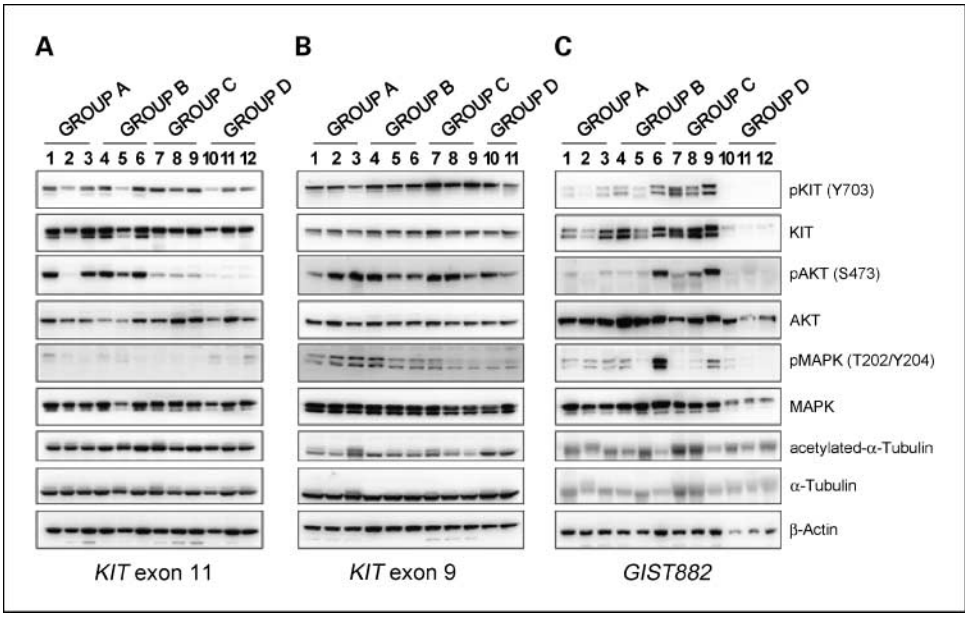

Fig. 5. Western analysis. Whole tissue lysates were used to assess total expression and phosphorylation of the KIT protein and its downstream molecules, AKT and MAPK. α-Tubulin acetylation has been assessed as a marker for the cytoplasmatic activity of LBH589.

overall an unexpected finding. For the GIST882-derived xenografts, this is in contradiction to our previous study showing loss of KIT phosphorylation in these xenografts under imatinib (27). The difference could relate to the use of passage 4 of these xenografts, which based on histology and tumor grow capacity show more aggressive biological features than previously (passage 0).

Interestingly, imatinib treatment also enhanced the H3 and H4 acetylation. This finding might be related to the inhibitory effect of imatinib on the RAS/MAPK pathway. Indeed, the constitutive activation of this pathway is associated with constitutive phosphorylation and translocation to the nucleus of HDAC4, one of the deacetylases associated with chromatin remodeling (39). Thus, inhibition of the RAS/MAPK pathway might prevent HDAC4 nuclear translocation.

Although we do not have statistical evidence for an enhanced effect of panobinostat-imatinib combination on tumor regression, we observed more prominent histopathologic changes than in single treatments, including higher apoptotic activity and histone acetylation. This is in line with a more recent *in vitro* study on GIST cell lines describing additive or synergistic effects of vorinostat, an HDACi in the same class with panobinostat, when combined with imatinib (19). Importantly, it is difficult to make a reliable comparison between the schedule/dose regimens adopted in our mouse study and the ones applied to human subjects in clinical trial. Indeed, panobinostat (LBH589) is still under early phase clinical trials in which the safety, tolerability, biological activity, and pharmacokinetic profile of panobinostat is currently studied.

One observation of our study was the loss of body weight under panobinostat, of up to 27%, which occurred most likely due to the treatment-induced diarrhea. The observed dysplastic megakariocytes in the spleen may explain the delayed healing of the petechiae in the abdominal wall. Diarrhea and thrombocytopenia were also reported as side effects in patients receiving HDACi (12, 18). As already observed in clinical trials, the inclusion of antidiarrhea treatment and alternative dose schedules (such as the three weekly oral administration) may improve the toxic profile of panobinostat leaving unaffected its therapeutic effects (40).

In conclusion, our results provide the first *in vivo* evidence for a potential therapeutic activity of HDACi in GIST. Panobinostat significantly induces necrosis, apoptosis, and arrest of tumor cell proliferation at variable degrees. In combination with imatinib, the described therapeutic effects were enhanced. The ability of panobinostat to synergize with, and potentially overcome resistance to, imatinib represents a promising strategy for the treatment of patients with advanced GISTs.

Disclosure of Potential Conflicts of Interest

P. Atadja, employment, Novartis Pharma; P. Schoffski, commercial research grant, Novartis; M. Debiec-Rychter, honoraria, Novartis Pharma.

Acknowledgments

We thank Dr. Bartosz Wasag for critical review of the discussion and Lieve Ophalvens and Kristel Vandenbroeck for their excellent technical assistance.

References

1. Rubin BP, Heinrich MC, Corless CL. Gastrointestinal stromal tumour. Lancet 2007;369:1731–41.
2. Miettinen M, Lasota J. Gastrointestinal stromal tumors: review on morphology, molecular pathology, prognosis, and differential diagnosis. Arch Pathol Lab Med 2006;130:1466–78.
3. Corless CL, Fletcher JA, Heinrich MC. Biology of gastrointestinal stromal tumors. J Clin Oncol 2004;22:3813–25.
4. Antonescu CR. Gastrointestinal stromal tumor (GIST) pathogenesis, familial GIST, and animal models. Semin Diagn Pathol 2006;23:63–9.
5. Lasota J, Miettinen M. KIT and PDGFRA mutations in gastrointestinal stromal tumors (GISTs). Semin Diagn Pathol 2006;23:91–102.
6. Sleijfer S, Wiemer E, Seynaeve C, Verweij J. Improved insight into resistance mechanisms to imatinib in gastrointestinal stromal tumors: a basis for novel approaches and individualization of treatment. Oncologist 2007;12:719–26.
7. Debiec-Rychter M, Cools J, Dumez H, et al. Mechanisms of resistance to imatinib mesylate in gastrointestinal stromal tumors and activity of the PKC412 inhibitor against imatinib-resistant mutants. Gastroenterology 2005;128:270–9.
8. Heinrich MC, Corless CL, Blanke CD, et al. Molecular correlates of imatinib resistance in gastrointestinal stromal tumors. J Clin Oncol 2006; 24:4764–74.
9. Fletcher JA, Rubin BP. KIT mutations in GIST. Curr Opin Genet Dev 2007;17:3–7.
10. Kostrouchova M, Kostrouch Z, Kostrouchova M. Valproic acid, a molecular lead to multiple regulatory pathways. Folia Biol (Praha) 2007;53: 37–49.
11. Johnstone RW. Histone-deacetylase inhibitors: novel drugs for the treatment of cancer. Nat Rev Drug Discov 2002;1:287–99.
12. Minucci S, Pelicci PG. Histone deacetylase inhibitors and the promise of epigenetic (and more) treatments for cancer. Nat Rev Cancer 2006;6:38–51.
13. Boyault C, Sadoul K, Pabion M, Khochbin S. HDAC6, at the crossroads between cytoskeleton and cell signaling by acetylation and ubiquitination. Oncogene 2007;26:5468–76.
14. Bali P, Pranpat M, Bradner J, et al. Inhibition of histone deacetylase 6 acetylates and disrupts the chaperone function of heat shock protein 90. J Biol Chem 2005;280:26729–34.
15. Yang Y, Rao R, Shen J, et al. Role of acetylation and extracellular location of heat shock protein 90α in tumor cell invasion. Cancer Res 2008; 68:4833–42.
16. Bauer S, Yu LK, Demetri GD, Fletcher JA. Heat shock protein 90 inhibition in imatinib-resistant gastrointestinal stromal tumor. Cancer Res 2006;66:9153–61.
17. Drummond DC, Noble CO, Kirpotin DB, Guo Z, Scott GK, Benz CC. Clinical development of histone deacetylase inhibitors as anticancer agents. Annu Rev Pharmacol Toxicol 2005;45:495–528.
18. Glaser KB. HDAC inhibitors: Clinical update and mechanism-based potential. Biochem Pharmacol 2007;74:659–71.
19. Muhlenberg T, Fletcher JA, Seeber S, Bauer S. Histone deacetylase-inhibitors in gastrointestinal stromal tumor (GIST): therapeutic potential. Proceedings of the AACR. 2007. Ref Type: Abstract.
20. Giles F, Fischer T, Cortes J, et al. A phase I study of intravenous LBH589, a novel cinnamic hydroxamic acid analogue histone deacetylase inhibitor, in patients with refractory hematologic malignancies. Clin Cancer Res 2006;12:4628–35.
21. Steele NL, Plumb JA, Vidal L, et al. A phase 1 pharmacokinetic and pharmacodynamic study of the histone deacetylase inhibitor belinostat in patients with advanced solid tumors. Clin Cancer Res 2008;14:804–10.
22. Gore L, Rothenberg ML, O'Bryant CL, et al. A phase I and pharmacokinetic study of the oral histone deacetylase inhibitor, MS-275, in patients with refractory solid tumors and lymphomas. Clin Cancer Res 2008;14:4517–25.
23. Siu LL, Pili R, Duran I, et al. Phase I study of MGCD0103 given as a three-times-per-week oral dose in patients with advanced solid tumors. J Clin Oncol 2008;26:1940–7.
24. Carey N, La Thangue NB. Histone deacetylase inhibitors: gathering pace. Curr Opin Pharmacol 2006;6:369–75.
25. Maiso P, Carvajal-Vergara X, Ocio EM, et al. The histone deacetylase inhibitor LBH589 is a potent antimyeloma agent that overcomes drug resistance. Cancer Res 2006;66:5781–9.
26. Tuveson DA, Willis NA, Jacks T, et al. STI571 inactivation of the gastrointestinal stromal tumor c-KIT oncoprotein: biological and clinical implications. Oncogene 2001;20:5054–8.
27. Prenen H, Deroose C, Vermaelen P, et al. Establishment of a mouse gastrointestinal stromal tumour model and evaluation of response to imatinib by small animal positron emission tomography. Anticancer Res 2006;26:1247–52.
28. Tomayko MM, Reynolds CP. Determination of subcutaneous tumor size in athymic (nude) mice. Cancer Chemother Pharmacol 1989;24: 148–54.
29. Agaram NP, Besmer P, Wong GC, et al. Pathologic and molecular heterogeneity in imatinib-stable or imatinib-responsive gastrointestinal stromal tumors. Clin Cancer Res 2007;13:170–81.

30. Debiec-Rychter M, Wasag B, Stul M, et al. Gastrointestinal stromal tumours (GISTs) negative for KIT (CD117 antigen) immunoreactivity. J Pathol 2004;202:430–8.
31. Sciot R, Debiec-Rychter M. GIST under imatinib therapy. Semin Diagn Pathol 2006;23:84–90.
32. Calnan DR, Brunet A. The FoxO code. Oncogene 2008;27:2276–88.
33. Seligson DB, Horvath S, Shi T, et al. Global histone modification patterns predict risk of prostate cancer recurrence. Nature 2005;435:1262–6.
34. Barlesi F, Giaccone G, Gallegos-Ruiz MI, et al. Global histone modifications predict prognosis of resected non small-cell lung cancer. J Clin Oncol 2007;25:4358–64.
35. Bolden JE, Peart MJ, Johnstone RW. Anticancer activities of histone deacetylase inhibitors. Nat Rev Drug Discov 2006;5:769–84.
36. Kruhlak MJ, Hendzel MJ, Fischle W, et al. Regulation of global acetylation in mitosis through loss of histone acetyltransferases and deacetylases from chromatin. J Biol Chem 2001;276:38307–19.
37. Lee YS, Lim KH, Guo X, et al. The cytoplasmic deacetylase HDAC6 is required for efficient oncogenic tumorigenesis. Cancer Res 2008;68:7561–69.
38. Liegl B, Kepten I, Le C, et al. Heterogeneity of kinase inhibitor resistance mechanisms in GIST. J Pathol 2008;216:64–74.
39. Zhou X, Richon VM, Wang AH, Yang XJ, Rifkind RA, Marks PA. Histone deacetylase 4 associates with extracellular signal-regulated kinases 1 and 2, and its cellular localization is regulated by oncogenic Ras. Proc Natl Acad Sci U S A 2000;97:14329–33.
40. Zhang L, Lebwohl D, Masson E, Laird G, Cooper MR, Prince HM. Clinically relevant QTc prolongation is not associated with current dose schedules of LBH589 (panobinostat). J Clin Oncol 2008;28:332–33.

Clinical Cancer Research

High Efficacy of Panobinostat Towards Human Gastrointestinal Stromal Tumors in a Xenograft Mouse Model

Giuseppe Floris, Maria Debiec-Rychter, Raf Sciot, et al.

Clin Cancer Res 2009;15:4066-4076.